The vortex gas scaling regime of baroclinic turbulence

Basile Gallet[a,1,2] **and Raffaele Ferrari**[b,1]

[a]Service de Physique de l'Etat Condensé, Commissariat à l'Energie Atomique Saclay, CNRS UMR 3680, Université Paris-Saclay, 91191 Gif-sur-Yvette, France; and [b]Department of Earth, Atmospheric and Planetary Sciences, Massachusetts Institute of Technology, Cambridge, MA 02139

Edited by William R. Young, University of California San Diego, La Jolla, CA, and approved January 15, 2020 (received for review September 20, 2019)

The mean state of the atmosphere and ocean is set through a balance between external forcing (radiation, winds, heat and freshwater fluxes) and the emergent turbulence, which transfers energy to dissipative structures. The forcing gives rise to jets in the atmosphere and currents in the ocean, which spontaneously develop turbulent eddies through the baroclinic instability. A critical step in the development of a theory of climate is to properly include the eddy-induced turbulent transport of properties like heat, moisture, and carbon. In the linear stages, baroclinic instability generates flow structures at the Rossby deformation radius, a length scale of order 1,000 km in the atmosphere and 100 km in the ocean, smaller than the planetary scale and the typical extent of ocean basins, respectively. There is, therefore, a separation of scales between the large-scale gradient of properties like temperature and the smaller eddies that advect it randomly, inducing effective diffusion. Numerical solutions show that such scale separation remains in the strongly nonlinear turbulent regime, provided there is sufficient drag at the bottom of the atmosphere and ocean. We compute the scaling laws governing the eddy-driven transport associated with baroclinic turbulence. First, we provide a theoretical underpinning for empirical scaling laws reported in previous studies, for different formulations of the bottom drag law. Second, these scaling laws are shown to provide an important first step toward an accurate local closure to predict the impact of baroclinic turbulence in setting the large-scale temperature profiles in the atmosphere and ocean.

oceanography | atmospheric dynamics | turbulence

Oceanic and atmospheric flows are subject to the combined effects of strong density stratification and rapid planetary rotation. On the one hand, these two ingredients add complexity to the dynamics, making the flow strongly anisotropic and inducing waves that modify the characteristics of the turbulent eddies. On the other hand, they permit the derivation of reduced sets of equations that capture the large-scale behavior of the flow: this is the realm of quasigeostrophy (QG). The outcome of this approach is a model that couples two-dimensional (2D) layers of fluid of different density. QG filters out fast-wave dynamics, relaxing the necessity to resolve the fastest timescales of the original system. A QG model with only two fluid layers is simple enough for fast and extensive numerical studies, and yet, it retains the key phenomenon arising from the combination of stable stratification and rapid rotation (1): baroclinic instability, with its ability to induce small-scale turbulent eddies from a large-scale vertically sheared flow. The two-layer quasigeostrophic (2LQG) model offers a testbed to derive and validate closure models for the "baroclinic turbulence" that results from this instability.

In the simplest picture of 2LQG, a layer of light fluid sits on top of a layer of heavy fluid, as sketched in Fig. 1*A*, in a frame rotating at a spatially uniform rate $\Omega = f/2$ around the vertical axis. Such a uniform Coriolis parameter f is a strong simplification compared with real atmospheres and oceans, where the β-effect associated with latitudinal variations in f can trigger the emergence of zonal jets. Nevertheless, β vanishes at the poles of a planet, and it seems that any global parameterization of baroclinic turbulence needs to correctly handle the limiting case $\beta = 0$, which we address in the present study. The 2LQG model applies to motions evolving on timescales long compared with the planetary rotation—the small Rossby number limit—and on horizontal scales larger than the equal depths of the two layers; refs. 2 and 3 provide more details on the derivation of QG. At leading order in Rossby number, the vertical momentum equation reduces to hydrostatic balance,* while the horizontal flow is in geostrophic balance.† These two balances imply that both the flow field and the local thickness of each layer can be expressed in terms of the corresponding stream functions, $\psi_1(x, y, t)$ in the upper layer and $\psi_2(x, y, t)$ in the lower layer. At the next order in Rossby number, the vertical vorticity equation yields the evolution equations for $\psi_1(x, y, t)$ and $\psi_2(x, y, t)$:

$$\partial_t q_1 + J(\psi_1, q_1) = -\nu\Delta^4 q_1, \qquad [1]$$

$$\partial_t q_2 + J(\psi_2, q_2) = -\nu\Delta^4 q_2 + \mathrm{drag}, \qquad [2]$$

where the subscripts 1 and 2 refer again to the upper and lower layers, respectively, and the Jacobian is $J(f, g) = \partial_x f \partial_y g - \partial_x g \partial_y f$. The potential vorticities $q_1(x, y, t)$ and $q_2(x, y, t)$ are related to the stream functions through

$$q_1 = \boldsymbol{\nabla}^2\psi_1 + \frac{1}{2\lambda^2}(\psi_2 - \psi_1), \qquad [3]$$

$$q_2 = \boldsymbol{\nabla}^2\psi_2 + \frac{1}{2\lambda^2}(\psi_1 - \psi_2), \qquad [4]$$

Significance

Developing a theory of climate requires an accurate parameterization of the transport induced by turbulent eddies. A major source of turbulence in the midlatitude planetary atmospheres and oceans is the baroclinic instability of the large-scale flows. We present a scaling theory that quantitatively predicts the local heat flux, eddy kinetic energy, and mixing length of baroclinic turbulence as a function of the large-scale flow characteristics and bottom friction. The theory is then used as a quantitative parameterization in the case of meridionally dependent forcing in the fully turbulent regime. Beyond its relevance for climate theories, our work is an intriguing example of a successful closure for a fully turbulent flow.

Author contributions: B.G. and R.F. designed research, performed research, analyzed data, and wrote the paper.

The authors declare no competing interest.

This article is a PNAS Direct Submission.

[1]B.G. and R.F. contributed equally to this work.

[2]To whom correspondence may be addressed. Email: basile.gallet@cea.fr.

This article contains supporting information online at https://www.pnas.org/lookup/suppl/doi:10.1073/pnas.1916272117/-/DCSupplemental.

First published February 18, 2020.

*Hydrostatic balance is the balance between the upward-directed pressure gradient force and the downward-directed force of gravity.

†Geostrophic balance is the balance between the Coriolis force and lateral pressure gradient forces.

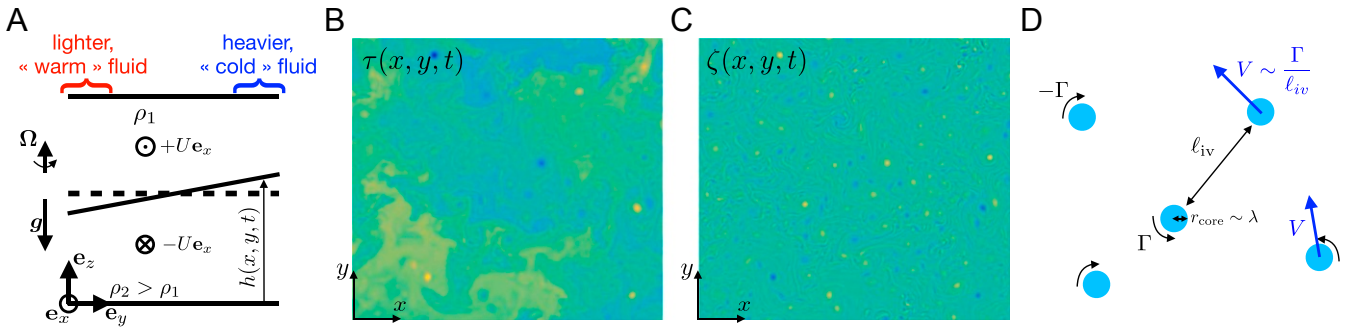

Fig. 1. (*A*) Base state of the 2LQG system with imposed vertical shear. The interface is tilted in the *y* direction as a consequence of thermal wind balance. The baroclinic stream function is proportional to $-h$, where $h(x, y, t)$ is the local displacement of the interface. For this reason, the baroclinic stream function is often referred to as the temperature field. Snapshots of the departure of the baroclinic stream function from the base state (τ; *B*) and of the barotropic vorticity (ζ; *C*) from a numerical simulation in the low-friction regime (arbitrary units; low values in dark blue, and large values in bright yellow). We model the barotropic flow as a gas of vortices (*D*) of circulation $\pm\Gamma$ and radius $r_{\mathrm{core}} \sim \lambda$. The vortex cores move as a result of their mutual interaction, with a typical velocity $V \sim \Gamma/\ell_{\mathrm{iv}}$, where ℓ_{iv} is the typical intervortex distance.

where λ denotes the Rossby deformation radius.[‡] In our model, the drag term is confined to the lower-layer Eq. **2**. In the case of linear drag, $\mathrm{drag} = -2\kappa\boldsymbol{\nabla}^2\psi_2$, and in the case of quadratic drag, $\mathrm{drag} = -\mu\,[\partial_x(|\boldsymbol{\nabla}\psi_2|\partial_x\psi_2) + \partial_y(|\boldsymbol{\nabla}\psi_2|\partial_y\psi_2)]$. Finally, Eqs. **1** and **2** include hyperviscosity to dissipate filaments of potential vorticity (enstrophy) generated by eddy stirring at small scales.

A more insightful representation arises from the sum and difference of Eqs. **1** and **2**: one obtains an evolution equation for the barotropic stream function—half the sum of the stream functions of both layers—which characterizes the vertically invariant part of the flow, and an evolution equation for the baroclinic stream function—half the difference between the two stream functions—which characterizes the vertically dependent flow. Because in QG the stream function is directly proportional to the thickness of the fluid layer, the baroclinic stream function is also a measure of the height of the interface between the two layers. A region with large baroclinic stream function corresponds to a locally deeper upper layer: there is more light fluid at this location, and we may thus say that on vertical average the fluid is warmer. Similarly, a region of low baroclinic stream function corresponds to a locally shallower upper layer, with more heavy fluid: this is a cold region. Thus, the baroclinic stream function is often denoted as τ and referred to as the local "temperature" of the fluid.

The 2LQG model can be used to study the equilibration of baroclinic instability arising from a prescribed horizontally uniform vertical shear, which represents the large-scale flows maintained by external forcing in the ocean and atmosphere. Denoting the vertical axis as z and the zonal and meridional directions as x and y, the prescribed flow in the upper and lower layers consists of zonal motion $+U\mathbf{e}_x$ and $-U\mathbf{e}_x$, respectively. This flow is in thermal wind balance[§] with a prescribed uniform meridional temperature gradient $-U$, i.e., there is a sloping interface between the heavy and light fluid layers (Fig. 1*A*). This tilt provides an energy reservoir, the available potential energy (APE) (4), that is released by baroclinic instability, acting to flatten the density interface. We denote, respectively, as $\psi(x, y, t)$ and $\tau(x, y, t)$ the perturbations of barotropic and baroclinic stream functions around this base state, and consider their evolution equations inside a large (horizontal) domain with periodic boundary conditions in both x and y:

$$\partial_t(\boldsymbol{\nabla}^2\psi) + J(\psi, \boldsymbol{\nabla}^2\psi) + J(\tau, \boldsymbol{\nabla}^2\tau) + U\partial_x(\boldsymbol{\nabla}^2\tau) \qquad [5]$$
$$= -\nu\boldsymbol{\nabla}^{10}\psi + \mathrm{drag}/2,$$

$$\partial_t[\boldsymbol{\nabla}^2\tau - \lambda^{-2}\tau] + J(\psi, \boldsymbol{\nabla}^2\tau - \lambda^{-2}\tau) + J(\tau, \boldsymbol{\nabla}^2\psi) \qquad [6]$$
$$+ U\partial_x[\boldsymbol{\nabla}^2\psi + \lambda^{-2}\psi] = -\nu\boldsymbol{\nabla}^8[\boldsymbol{\nabla}^2\tau - \lambda^{-2}\tau] - \mathrm{drag}/2.$$

The system releases APE by developing eddy motion through baroclinic instability, and the goal is to characterize the statistically steady turbulent state that ensues. How energetic is the barotropic flow? How strong are the local temperature fluctuations? Most importantly, what is the eddy-induced meridional heat flux? The latter quantity is a key missing ingredient required to formulate a theory of the mean state of the atmosphere and ocean as a function of external forcing parameters (5).

Traditionally, these questions have been addressed using descriptions of the flow in spectral space, focusing on the cascading behavior of the various invariants (6). In contrast with this approach, Thompson and Young (7) describe the system in physical space and argue that the barotropic flow evolves toward a gas of isolated vortices. Despite this intuition, Thompson and Young (7) cannot derive the scaling behavior of the quantities mentioned above and resort to empirical fits instead. Focusing on the case of linear drag, they conclude that the temperature fluctuations and meridional heat flux are extremely sensitive to the drag coefficient: they scale exponentially in inverse drag coefficient. This scaling dependence was recently shown by Chang and Held (8) to change if linear drag is replaced by quadratic drag: the exponential dependence becomes a power law dependence on the drag coefficient. However, Chang and Held (8) acknowledge the failure of standard cascade arguments to predict the exponents of these power laws, and they resort to curve fitting as well.

In this work, we supplement the vortex gas approach of Thompson and Young (7) with statistical arguments from point vortex dynamics to obtain a predictive scaling theory for the eddy kinetic energy, the temperature fluctuations, and the meridional heat flux of baroclinic turbulence. The resulting scaling theory captures both the exponential dependence of these quantities on the inverse linear drag coefficient and their power law dependence on the quadratic drag coefficient. Our predictions are thus in quantitative agreement with the scaling laws diagnosed empirically by both Thompson and Young (7) and Chang and Held (8). Following Pavan and Held (9) and Chang and Held (8), we finally show how these scaling laws can be used as a quantitative turbulent closure to make analytical predictions in

[‡] The Rossby radius of deformation λ is the length scale at which rotational effects become as important as buoyancy or gravity wave effects in the evolution of a flow.

[§] A flow in thermal wind balance satisfies both hydrostatic and geostrophic balance.

situations where the system is subject to inhomogeneous forcing at large scale.

The QG Vortex Gas

Denoting as $\langle\cdot\rangle$ a spatial and time average and as $\psi_x = \partial_x \psi$ the meridional barotropic velocity, our goal is to determine the meridional heat flux $\langle \psi_x \tau \rangle$, or equivalently, the diffusivity $D = \langle \psi_x \tau \rangle / U$ that connects this heat flux to minus the background temperature gradient U. A related quantity of interest is the mixing length $\ell = \sqrt{\langle \tau^2 \rangle}/U$. This is the typical distance traveled by a fluid element carrying its background temperature before it is mixed with the environment and relaxes to the local background temperature. It follows that the typical temperature fluctuations around the background gradient are of the order of $U\ell$. We seek the dependence of D and ℓ on the various external parameters of the system. It was established by Thompson and Young (7) that, for a sufficiently large domain, the mixing length saturates at a value much smaller than the domain size and independent of it. The consequence is that the size of the domain is irrelevant for large-enough domains. The small-scale dissipation coefficient—a hyperviscosity in most studies—is also shown by Thompson and Young (7) to be irrelevant when low enough. The quantities D and ℓ thus depend only on the dimensional parameters U, the Rossby deformation radius λ, and the bottom drag coefficient denoted as κ in the case of linear friction (with dimension of an inverse time) and as μ in the case of quadratic drag (with dimension of an inverse length) (8, 10). In dimensionless form, we thus seek the dependence of the dimensionless diffusivity $D_* = D/U\lambda$ and mixing length $\ell_* = \ell/\lambda$ on the dimensionless drag $\kappa_* = \kappa\lambda/U$ or $\mu_* = \mu\lambda$.

We follow the key intuition of Thompson and Young (7) that the flow is better described in physical space than in spectral space. In Fig. 1, we provide snapshots of the barotropic vorticity and baroclinic stream function from a direct numerical simulation in the low-drag regime (the numerical methods are in *SI Appendix*): the barotropic flow consists of a "gas" of well-defined vortices, with a core radius substantially smaller than the intervortex distance ℓ_{iv}. Vortex gas models were introduced to describe decaying 2D (purely barotropic) turbulence. It was shown that the time evolution of the gross vortex statistics, such as the typical vortex radius and circulation, can be captured using simpler "punctuated Hamiltonian" models (11–13). The latter consist of integrating the Hamiltonian dynamics governing the interaction of localized compact vortices (14), interrupted by instantaneous merging events when two vortices come close enough to one another, with specific merging rules governing the strength and radius of the vortex resulting from the merger. These models were adapted to the forced dissipative situation by Weiss (15) through injection of small vortices with a core radius comparable with the injection scale and removal of the largest vortices above a cutoff vortex radius. The resulting model captures the statistically steady distribution of vortex core radius observed in direct numerical simulations of the 2D Navier–Stokes equations (16): $P(r_{\rm core}) \sim r_{\rm core}^{-4}$ for $r_{\rm core}$ above the injection scale. One immediate consequence of such a steeply decreasing distribution function is that the mean vortex core radius is comparable with the injection scale. Similarly, the average vortex circulation is dominated by the circulation of the injected vortices. In the following, we will thus infer the transport properties of the barotropic component of the two-layer model by focusing on an idealized vortex gas consisting of vortices with a single "typical" value of the vortex core radius $r_{\rm core}$ comparable with the injection scale and circulations $\pm\Gamma$, where Γ is the typical magnitude of the vortex circulation. For baroclinic turbulence, both linear stability analysis (2, 3) and the multiple cascade picture (6) indicate that the barotropic flow receives energy at a scale comparable with the deformation radius λ. As discussed above, the typical vortex core radius is comparable with this injection scale, and we obtain $r_{\rm core} \sim \lambda$. We stress the fact that such a small core radius is fully compatible with the phenomenology of the inverse energy cascade: inverse energy transfers result in the vortices being farther apart, with little increase in core radius. The resulting velocity structures have a scale comparable with the large intervortex distance, even though the intense vortices visible in the vorticity field have a small core radius, comparable with the injection scale. Finally, it is worth noting that there is encouraging observational evidence both in the atmosphere and ocean that eddies have a core radius close to the scale at which they are generated through baroclinic instability (17, 18).

A schematic of the resulting idealized vortex gas is provided in Fig. 1*D*: we represent the barotropic flow as a collection of vortices of circulation $\pm\Gamma$ and of core radius $r_{\rm core} \sim \lambda$, and thus, a velocity decaying as $\pm\Gamma/r$ outside the core (19). The vortices move as a result of their mutual interactions, with a typical velocity $V \sim \Gamma/\ell_{iv}$. Through this vortex gas picture, we have introduced two additional parameters $\ell_{\rm iv}$ and V—or alternatively, $\Gamma = \ell_{\rm iv} V$—for a total of five parameters: D, ℓ, $\ell_{\rm iv}$, V, and a drag coefficient (κ or μ). We thus need four relations between these five quantities to produce a fully closed scaling theory.

The first of these relations is the energy budget: the meridional heat flux corresponds to a rate of release of APE, $U\langle\psi_x\tau\rangle/\lambda^2 = DU^2/\lambda^2$, which is balanced by frictional dissipation of kinetic energy in statistically steady state. The contribution from the barotropic flow dominates this frictional dissipation in the low-drag asymptotic limit, and the energy power integral reads [e.g., Thompson and Young (7)] (*SI Appendix*)

$$\frac{DU^2}{\lambda^2} = \begin{cases} \kappa \left\langle \mathbf{u}^2 \right\rangle & \text{for linear drag}, \\ \frac{\mu}{2} \left\langle |\mathbf{u}|^3 \right\rangle & \text{for quadratic drag}, \end{cases} \qquad [7]$$

where $\mathbf{u} = -\boldsymbol{\nabla} \times (\psi\, \mathbf{e}_z)$ denotes the barotropic velocity field. Our approach departs from both Thompson and Young (7) and Chang and Held (8) in the way that we evaluate the velocity statistics that appear on the right-hand side: we argue that a key aspect of vortex gas dynamics is that the various velocity moments scale differently and cannot be estimated simply as V above. Indeed, consider a single vortex within the vortex gas. It occupies a region of the fluid domain of typical extent $\ell_{\rm iv}$. The vorticity is contained inside a core of radius $r_{\rm core} \sim \lambda \ll \ell_{\rm iv}$, and the barotropic velocity $\mathbf{u}$ has a magnitude $\Gamma/2\pi r$ outside the vortex core, where r is the distance to the vortex center. The velocity variance is thus

$$\left\langle \mathbf{u}^2 \right\rangle = \frac{1}{\pi \ell_{\rm iv}^2} \int_{r_{\rm core}}^{\ell_{\rm iv}} \frac{\Gamma^2}{4\pi^2 r^2}\, 2\pi r {\rm d}r \sim V^2 \log\left(\frac{\ell_{\rm iv}}{\lambda}\right). \qquad [8]$$

This estimate for $\left\langle \mathbf{u}^2 \right\rangle$ exceeds that of Thompson and Young (7) by a logarithmic correction that captures the fact that the velocity is strongest close to the core of the vortex. This correction will turn out to be crucial to obtain the right scaling behaviors for D_* and ℓ_*. In a similar fashion, we estimate the third-order moment of the barotropic velocity field as

$$\left\langle |\mathbf{u}|^3 \right\rangle = \frac{1}{\pi \ell_{\rm iv}^2} \int_{r_{\rm core}}^{\ell_{\rm iv}} \frac{\Gamma^3}{8\pi^3 r^3}\, 2\pi r {\rm d}r \sim V^3\, \frac{\ell_{\rm iv}}{\lambda}, \qquad [9]$$

where we have used the fact that $r_{\rm core} \sim \lambda \ll \ell_{\rm iv}$. Again, this estimate exceeds that of Chang and Held (8) by the factor $\ell_{\rm iv}/\lambda$, a correction that arises from the vortex gas nature of the flow field.

The next steps of the scaling theory are common to linear and quadratic drag. As in any mixing-length theory, we will

express the diffusion coefficient D as the product of the mixing length and a typical velocity scale. In the vortex gas regime, one can anticipate that the mixing length ℓ scales as the typical intervortex distance ℓ_{iv}, an intuition that will be confirmed by Eq. **11** below. However, a final relationship for the relevant velocity scale is more difficult to anticipate as we have seen that the various barotropic velocity moments scale differently. The goal is thus to determine this velocity scale through a precise description of the transport properties of the assembly of vortices.

Stirring of a tracer like temperature takes place at scales larger than the stirring rods: in our problem, the vortices of size λ. At scales much larger than λ, the τ-equation [**6**] reduces to (7, 20, 21)

$$\partial_t \tau + J(\psi, \tau) = U\psi_x - \nu\Delta^4\tau. \qquad \textbf{[10]}$$

$U\psi_x$ represents the generation of τ-fluctuations through stirring of the large-scale temperature gradient $-U$, and the Jacobian term represents the advection of τ-fluctuations by the barotropic flow. Eq. **10** is thus that of a passive scalar with an externally imposed uniform gradient $-U$ stirred by the barotropic flow. To check the validity of this analogy, we have implemented such passive tracer dynamics into our numerical simulations: in addition to solving Eqs. **5** and **6**, we solve Eq. **10** with τ replaced by the concentration c of a passive scalar and $-U$ replaced by an imposed meridional gradient $-G_c$ of scalar concentration. In the low-drag simulations, the resulting passive scalar diffusivity $D_c = \langle \psi_x c \rangle / G_c$ equals the temperature diffusivity D within a few percent, whereas D is significantly lower than D_c for larger drag, when the intervortex distance becomes comparable with λ. This validates our assumption that the diffusivity is mostly due to flow structures larger than λ in the low-drag regime, the impact of which on the temperature field is accurately captured by the approximate Eq. **10**. We can thus safely build intuition into the behavior of the temperature field by studying Eq. **10**.

A natural first step would be to compute the heat flux associated with a single steady vortex. However, this situation turns out to be rather trivial: the vortex stirs the temperature field along closed circles until it settles in a steady state that has a vanishing projection onto the source term $U\psi_x$, and the resulting heat flux $\langle \psi_x \tau \rangle$ vanishes up to hyperviscous corrections. Instead of a single steady vortex, the simplest heat-carrying configuration is a vortex dipole, such as the one sketched in Fig. 2*A*: two vortices of opposite circulations $\pm\Gamma$ are separated by a distance ℓ_{iv} much larger than their core radius $r_{\text{core}} \sim \lambda$. This dipole mimics the two nearest vortices of any given fluid element, which we argue is a sufficient model to capture the qualitative transport properties of the entire vortex gas. Without loss of generality, the vortices are initially aligned along the zonal axis, and as a result of their mutual interaction, they travel in the y direction at constant velocity $\Gamma/2\pi\ell_{iv}$. For the configuration sketched in Fig. 2*A*, the meridional velocity is positive between the two vortices and becomes negative at both ends of the dipole. For positive U, this corresponds to a heat source between the vortices and two heat sinks away from the dipole. These heat sources and sinks are positively correlated with the local meridional barotropic velocity so that there is a net meridional heat flux $\langle \psi_x \tau \rangle$ associated with this configuration. We have integrated numerically Eq. **10** for this moving dipole over a time ℓ_{iv}/V, which corresponds to the time needed for the dipole to travel a distance ℓ_{iv}. This is the typical distance traveled by these two vortices before pairing up with other vortices inside the gas. Fig. 2 *C* and *D* shows the resulting temperature field and local flux $\psi_x\tau$ at the end of the numerical integration (*SI Appendix* has details). A suite of numerical simulations for such dipole configurations indicates that, at the end time of the numerical integration, the local mixing length and diffusivity obey the scaling relations:

$$\ell \sim \ell_{iv}, \qquad \textbf{[11]}$$

$$D \sim \ell_{iv}\, V, \qquad \textbf{[12]}$$

while the variance and third-order moment of the vortex dipole flow field satisfy [**8**] and [**9**] at every time. It is interesting that the velocity scale arising in the diffusivity [**12**] is V and not the rms velocity $\langle \mathbf{u}^2 \rangle^{1/2}$. This is because the fluid elements that are trapped in the immediate vicinity of the vortex cores do not carry heat, in a similar fashion that a single vortex is unable to transport heat. Only the fluid elements located at a fraction of ℓ_{iv} away from the vortex centers carry heat, and these fluid elements have a typical velocity V.

The relations [**11**] and [**12**] hold for any passive tracer. However, temperature is an active tracer so that the velocity scale in turn depends on the temperature fluctuations, providing the fourth scaling relation. This relation can be derived through a simple heuristic argument: consider a fluid particle, initially at rest, that accelerates in the meridional direction by transforming potential energy into barotropic kinetic energy by flattening the density interface as a result of baroclinic instability. In line with the standard assumptions of a mixing-length model, we assume that the fluid particle travels in the meridional direction over a distance ℓ before interacting with the other fluid particles. Balancing the kinetic energy gained over the distance ℓ with the difference in potential energy between two fluid columns a distance ℓ apart, we obtain the final barotropic velocity of the fluid element: $v_f \sim U\ell/\lambda$. This velocity estimate does not hold for the particles that rapidly loop around a vortex center, with little changes in APE; it holds only for the fluid elements that travel in the meridional direction, following a somewhat straight

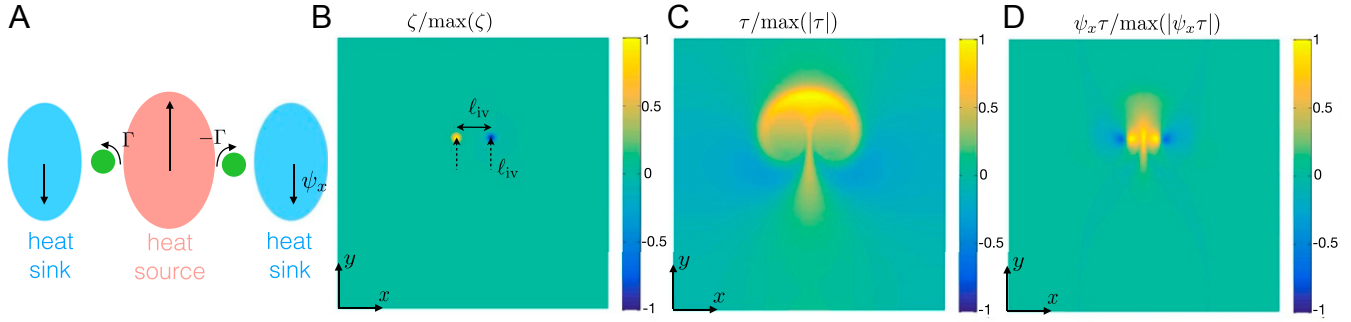

Fig. 2. Heat transport by a barotropic vortex dipole. *A* is a schematic representation of the heat sources and sinks induced by the dipolar velocity field. *B–D* show the barotropic vorticity, temperature field, and local meridional heat flux, respectively, at the end time of a numerical solution of [**10**] where the dipole travels over a distance ℓ_{iv} in the meridional direction y.

trajectory (these fluid elements happen to be the ones that carry heat according to the dipole model described above). Such fluid elements have a typical velocity V, which we identify with v_f to obtain

$$V \sim U\ell/\lambda. \qquad [13]$$

A similar relation was derived by Green (22), who computes the kinetic energy gained by flattening the density interface over the whole domain. In the present periodic setup, the mean slope of the interface is imposed, and the estimate [**13**] holds locally for the heat-carrying fluid elements traveling a distance ℓ instead. The estimate [**13**] is also reminiscent of the "free-fall" velocity estimate of standard upright convection, where the velocity scale is estimated as the velocity acquired during a free fall over one mixing length (23–25). The conclusion is that the typical velocity is directly proportional to the mixing length. The baroclinic instability is sometimes referred to as slantwise convection, and the velocity estimate [**13**] is the corresponding "slantwise free-fall" velocity. To validate [**13**], one can notice that, when combined with [**11**] and [**12**], it leads to the simple relation

$$D_* \sim \ell_*^2. \qquad [14]$$

Anticipating the numerical results presented in Fig. 3, this relation is well satisfied in the dilute low-drag regime, $\ell \gtrsim 10\lambda$, with the solid lines in Fig. 3 being precisely related by [**14**] above. A relation very close to [**14**] was reported by Larichev and Held (21) using turbulent cascade arguments. Their relation is written in terms of an "energy-containing wavenumber" instead of a mixing length. If this energy-containing wavenumber is interpreted to be the inverse intervortex distance of the vortex gas model, then their relation becomes identical to [**14**].

The four relations needed to establish the scaling theory are [**7**] and [**11**]–[**13**]. In the case of linear drag, their combination leads to $\log(\ell_*) \sim 1/\kappa_*$ or simply,

$$\ell_* = c_1 \exp\left(\frac{c_2}{\kappa_*}\right), \qquad [15]$$

where c_1 and c_2 are dimensionless constants. The vortex gas approach thus provides a clear theoretical explanation to the exponential dependence of ℓ on inverse drag reported by Thompson and Young (7), which is shown to stem from the logarithmic factor in [**8**] for the dissipation of kinetic energy. It is remarkable that these authors could extract the correct functional dependence of ℓ_* with κ_* from their numerical simulations. We have performed similar numerical simulations in large-enough domains to avoid finite-size effects and at low-enough hyperviscosity to neglect hyperdissipation in the kinetic energy budget. The numerical implementation of the equations as well as the parameter values of the various numerical runs are provided in *SI Appendix*. In Fig. 3, we plot ℓ_* as a function of κ_*. We obtain an excellent agreement between the asymptotic prediction [**15**] and our numerical data using $c_1 = 3.2$ and $c_2 = 0.36$. The dimensionless diffusivity is deduced from ℓ_* using the relation [**14**], which leads to

$$D_* = c_3 \exp\left(\frac{2c_2}{\kappa_*}\right). \qquad [16]$$

Once again, on choosing $c_3 = 1.85$, this expression is in excellent agreement with the numerical data (Fig. 3).

When linear friction is replaced by quadratic drag, only the energy budget [**7**] is modified. As can be seen in Eq. **9**, the main difference is that quadratic drag operates predominantly in the vicinity of the vortex cores, which has a direct impact on the scaling behaviors of ℓ_* and D_*. Indeed, combining [**7**] and [**11**]–[**13**] yields

$$\ell_* = \frac{c_4}{\sqrt{\mu_*}}, \qquad [17]$$

which, using [**14**], leads to the diffusivity

$$D_* = \frac{c_5}{\mu_*}. \qquad [18]$$

Using the values $c_4 = 2.62$ and $c_5 = 2.0$, the predictions are again in very good agreement with the numerical data, although the convergence to the asymptotic prediction for D_* seems somewhat slower for this configuration (Fig. 3).

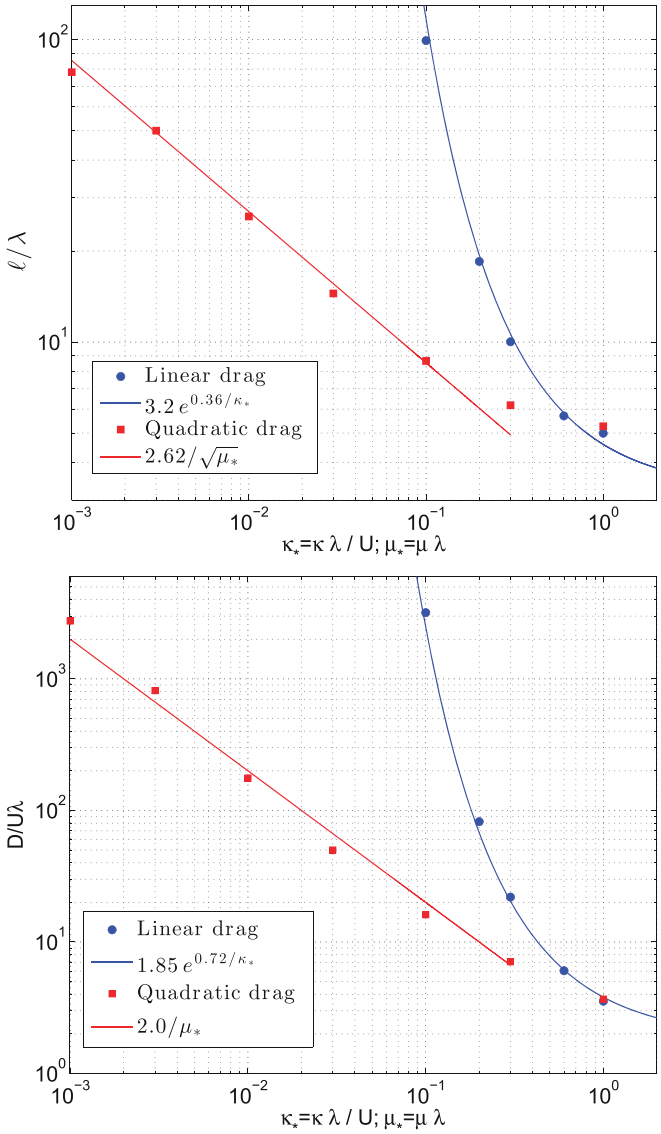

Fig. 3. Dimensionless mixing length ℓ_* and diffusivity D_* as functions of dimensionless drag for both linear and quadratic drag. Symbols correspond to numerical simulations, while the solid lines are the predictions [**15**–**18**] from the vortex gas scaling theory.

Using These Scaling Laws as a Local Closure

We now wish to demonstrate the skill of these scaling laws as local diffusive closures in situations where the heat flux and the temperature gradient have some meridional variations. For simplicity, we consider an imposed heat flux with a sinusoidal dependence in the meridional direction y. The modified governing equations for the potential vorticities $q_{1;2}$ of each layer are

$$\partial_t q_1 + J(\psi_1, q_1) = Q \sin(y/L) - \nu\Delta^4 q_1, \qquad [19]$$

$$\partial_t q_2 + J(\psi_2, q_2) = -Q\sin(y/L) - \nu\Delta^4 q_2 + \text{drag}. \qquad [20]$$

It becomes apparent that the Q terms represent a heat flux when the governing equations are written for the (total) baroclinic and barotropic stream functions τ and ψ: the τ-equation, obtained by subtracting **[20]** from **[19]** and dividing by two, has a source term $Q\sin(y/L)$ that forces some meridional temperature structure. By contrast, the ψ-equation obtained by adding **[19]** and **[20]** has no source terms. The goal is to determine the temperature profile associated with the imposed meridionally dependent heat flux. This slantwise convection forced by sources and sinks is somewhat similar to standard upright convection forced by sources and sinks of heat (26, 27). We focus on the statistically steady state by considering a zonal and time average denoted as $\overline{\cdot}$. Neglecting the dissipative terms, the average of both Eqs. **19** and **20** leads to

$$Q\sin(y/L) = -\frac{1}{\lambda^2}\partial_y\overline{\psi_x\tau}. \qquad [21]$$

Provided that the imposed heat flux varies on a scale L much larger than the local mixing length ℓ, we can relate the local flux $\overline{\psi_x\tau}(y)$ to the local temperature gradient $U(y) = -\partial_y\overline{\tau}$ by the diffusive relation $\overline{\psi_x\tau}(y) = DU(y) = D_*\lambda|U(y)|U(y)$. In the case of quadratic drag, inserting this relation into **[21]** and substituting the scaling law **[18]** for $D_*(\mu_*)$ yields

$$-\frac{c_5}{\mu_*}\partial_y\left[|\partial_y\overline{\tau}|\partial_y\overline{\tau}\right] = Q\sin(y/L). \qquad [22]$$

In terms of the dimensionless temperature $\tau_* = \tau/\lambda^2\sqrt{Q}$, the solution to this equation is

$$\overline{\tau}_*(y/L) = 2\left(\frac{L}{\lambda}\right)^{3/2}\sqrt{\frac{\mu_*}{c_5}}\,\mathcal{E}\left(\frac{y}{2L}|2\right), \qquad [23]$$

where $\mathcal{E}$ denotes the incomplete elliptic integral of the second kind. Expression **[23]** holds for $y/L \in [-\pi/2; \pi/2]$, the entire graph being easily deduced from the fact that $\overline{\tau}_*(y/L)$ is symmetric to a translation by π accompanied by a sign change.

In the case of linear drag, we substitute the scaling law **[16]** for $D_*(\kappa_*) = D_*(\lambda\kappa/|\partial_y\overline{\tau}|)$ instead. The integration of the resulting ordinary differential equation yields the dimensionless temperature profile:

$$\overline{\tau}_*(y/L) = \frac{\kappa L}{c_2\lambda\sqrt{Q}}\int_0^{y/L}\mathcal{W}\left(\frac{c_2}{\kappa}\sqrt{\frac{LQ}{c_3\lambda}\cos s}\right)\mathrm{d}s, \qquad [24]$$

where $\mathcal{W}$ denotes the Lambert function. Once again, **[24]** holds for $y/L \in [-\pi/2; \pi/2]$, the entire graph being easily deduced from the fact that $\overline{\tau}_*(y/L)$ is symmetric to a translation by π accompanied by a sign change.

To test these theoretical predictions, we solved numerically Eqs. **19** and **20** inside a domain $(x, y) \in [0; 2\pi L]^2$ with periodic boundary conditions for both linear and quadratic drag. We compute the time and zonally averaged temperature profiles and compare them with the theoretical predictions using the values of the parameters $c_{1;2;3;4;5}$ deduced above. In Fig. 4, we show snapshots of the temperature field in statistically steady state together with meridional temperature profiles. The predictions **[23]** and **[24]** are in excellent agreement with the numerical results for both linear and quadratic drag, and this good agreement holds provided the various length scales of the problem are ordered in the following fashion: $\lambda \ll \ell \ll L$. The first inequality corresponds to the dilute vortex gas regime for which the scaling theory is established, while the second inequality is the scale separation required for any diffusive closure to hold. For fixed L/λ, the first inequality breaks down at large friction, $\kappa_* \sim 1$ or $\mu_* \sim 1$, where the system becomes a closely packed "vortex liquid" (10, 28). The second inequality breaks down at low friction when $\ell \sim L$. From the scaling laws **[15]** and **[17]**, this loss of scale separation occurs for $\kappa_* \lesssim 1/\log(L/\lambda)$ and $\mu_* \lesssim (\lambda/L)^2$ for linear and quadratic drag, respectively.

Discussion

The vortex gas description of baroclinic turbulence allowed us to derive predictive scaling laws for the dependence of the mixing length and diffusivity on bottom friction and to capture the key differences between linear and quadratic drag. The scaling behavior of the diffusivity of baroclinic turbulence seems more "universal" than that of its purely barotropic counterpart. This is likely because many different mechanisms are used in the literature to drive purely barotropic turbulence. For instance, the power input by a steady sinusoidal forcing (29, 30) strongly differs from that input by forcing with a finite (31) or vanishing (32) correlation time, with important consequences for the large-scale properties and diffusivity of the resulting flow. By contrast, baroclinic turbulence comes with its own injection mechanism—baroclinic instability—and the resulting scaling laws depend only on the form of the drag. We demonstrated the skills of these scaling laws when used as local parameterizations of the turbulent heat transport in situations where the large-scale forcing is inhomogeneous. While this theory provides some qualitative understanding of turbulent heat transport in planetary

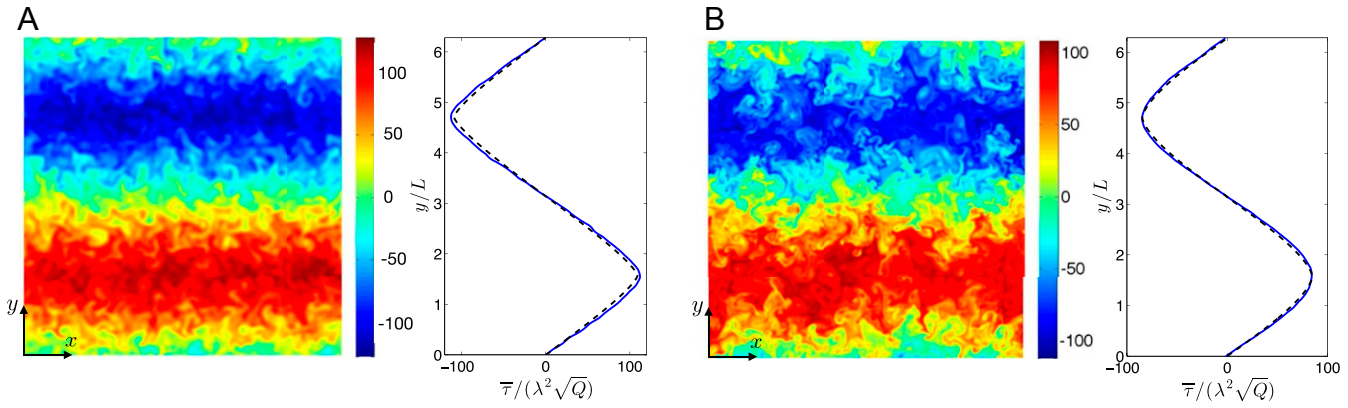

Fig. 4. Testing the diffusive closure. Snapshots and meridional profiles of the dimensionless temperature $\tau/\lambda^2 Q^{1/2}$. The solid lines are the zonal and time mean from the numerical simulations, while the dashed lines are the theoretical expressions **[23]** and **[24]**. (*A*) Linear drag, with $\kappa/Q^{1/2} = 0.5$ and $\lambda/L = 0.02$. (*B*) Quadratic drag, with $\mu_* = 10^{-2}$ and $\lambda/L = 0.01$.

atmospheres, it should be recognized that the scale separation is at best moderate in Earth atmosphere, where meridional changes in the Coriolis parameter also drive intense jets. However, our firmly footed scaling theory could be the starting point to a complete parameterization of baroclinic turbulence in the ocean, a much-needed ingredient of global ocean models. Along the path, one would need to adapt the present approach to models with multiple layers, possibly going all of the way to a geostrophic model with continuous density stratification or even back to the primitive equations. The question would then be whether the vortex gas provides a good description of the equilibrated state in these more general settings. Even more challenging would be the need to include additional physical ingredients in the scaling theory: the meridional changes in f mentioned above, but also variations in bottom topography and surface wind stress. Whether the vortex gas approach holds in those cases will be the topic of future studies.

Data Availability. The data associated with this study are available within the paper and *SI Appendix*.

ACKNOWLEDGMENTS. Our work is supported by Eric and Wendy Schmidt by recommendation of the Schmidt Futures Program and by NSF Grant AGS-6939393. This research is also supported by European Research Council Grant FLAVE 757239.

1. G. R. Flierl, Models of vertical structure and the calibration of two-layer models. *Dyn. Atmos. Oceans* **2**, 342–381 (1978).
2. R. Salmon, *Lectures on Geophysical Fluid Dynamics* (Oxford University Press, 1998).
3. G. K. Vallis, *Atmospheric and Oceanic Fluid Dynamics: Fundamentals and Large-Scale Circulation* (Cambridge University Press, 2006).
4. E. N. Lorenz, Available potential energy and the maintenance of the general circulation. *Tellus* **7**, 157–167 (1955).
5. I. M. Held, The macroturbulence of the troposphere. *Tellus* **51A-B**, 59–70 (1999).
6. R. Salmon, Two-layer quasigeostrophic turbulence in a simple special case. *Geophys. Astrophys. Fluid Dyn.* **10**, 25–52 (1978).
7. A. F. Thompson, W. R. Young, Scaling baroclinic eddy fluxes: Vortices and energy balance, *J. Phys. Oceanogr.* **36**, 720–736 (2005).
8. C.-Y. Chang, I. M. Held, The control of surface friction on the scales of baroclinic eddies in a homogeneous quasigeostrophic two-layer model. *J. Atmospheric Sci.* **76**, 1627–1643 (2019).
9. V. Pavan, I. M. Held, The diffusive approximation for eddy fluxes in baroclinically unstable jets. *J. Atmospheric Sci.* **53**, 1262–1272 (1996).
10. B. K. Arbic, R. B. Scott, On quadratic bottom drag, geostrophic turbulence, and oceanic mesoscale eddies. *J. Phys. Oceanogr.* **38**, 84–103 (2007).
11. G. F. Carnevale, J. C. McWilliams, Y. Pomeau, J. B. Weiss, W. R. Young, Evolution of vortex statistics in two-dimensional turbulence. *Phys. Rev. Lett.* **66**, 2735–2737 (1991).
12. J. B. Weiss, J. C. McWilliams, Temporal scaling behavior of decaying two-dimensional turbulence. *Phys. Fluids A* **5**, 608–621 (1993).
13. E. Trizac, A coalescence model for freely decaying two-dimensional turbulence. *Europhys. Lett.* **43**, 671–676 (1998).
14. L. Onsager, Statistical hydrodynamics. *Nuovo Cimento* **6** (suppl. 2), 279–287 (1949).
15. J. B. Weiss, "Punctuated Hamiltonian models of structured turbulence" in *Semi-Analytic Methods for the Navier–Stokes Equations*, K. Coughlin, Ed. (Centre de Recherches Mathématiques, Proceedings & Lecture Notes, American Mathematical Society, Providence, RI, 1999), vol. 20, pp. 109–119.
16. V. Borue, Inverse energy cascade in stationary two-dimensional homogeneous turbulence. *Phys. Rev. Lett.* **72**, 1475–1478 (1994).
17. T. Schneider, C. C. Walker, Self-organization of atmospheric macroturbulence into critical states of weak nonlinear eddy-eddy interactions. *J. Atmospheric Sci.* **63**, 1569–1586 (2006).
18. R. Tulloch, J. Marshall, C. Hill, K. S. Smith, Scales, growth rates, and spectral fluxes of baroclinic instability in the ocean. *J. Phys. Oceanogr.* **41**, 1057–1076 (2011).
19. J. G. Charney, "Numerical experiments in atmospheric hydrodynamics" in *Experimental Arithmetic, High Speed Computing and Mathematics, Proceedings of Symposia in Applied Mathematic*, N. C. Metropolis, A. H. Taub, J. Todd, C. B. Tompkins, Eds. (American Mathematical Society, Providence, RI, 1963), vol. 15, pp. 289–310.
20. R. Salmon, Baroclinic instability and geostrophic turbulence. *Geophys. Astrophys. Fluid Dyn.* **15**, 157–211 (1980).
21. V. Larichev, I. M. Held, Eddy amplitudes and fluxes in a homogeneous model of fully developed baroclinic instability, *J. Phys. Oceanogr.* **25**, 2285–2297 (1995).
22. J. S. A. Green, Transfer properties of the large-scale eddies and the general circulation of the atmosphere. *Quart. J. R. Met. Soc.* **96**, 157–185 (1970).
23. E. A. Spiegel, A generalization of the mixing-length theory of thermal convection. *Astrophys. J.* **138**, 216 (1963).
24. E. A. Spiegel, Convection in stars. I. Basic Boussinesq convection. *Annu. Rev. Astron. Astrophys.* **9**, 323–352 (1971).
25. M. Gibert *et al.*, High-Rayleigh-Number convection in a vertical channel. *Phys. Rev. Lett.* **96**, 084501 (2006).
26. S. Lepot, S. Aumaître, B. Gallet, Radiative heating achieves the ultimate regime of thermal convection. *Proc. Nat. Acad. Sci. U.S.A.* **115**, 8937–8941 (2018).
27. V. Bouillaut, S. Lepot, S. Aumaître, B. Gallet, Transition to the ultimate regime in a radiatively driven convection experiment. *J. Fluid Mech.* **861**, R5 (2019).
28. B. K. Arbic, G. R. Flierl, Baroclinically unstable geostrophic turbulence in the limits of strong and weak bottom Ekman friction: Application to midocean eddies. *J. Phys. Oceanogr.* **34**, 2257–2273 (2004).
29. Y.-K. Tsang, W. R. Young, Forced-dissipative two-dimensional turbulence: A scaling regime controlled by drag. *Phys. Rev. E* **79**, 045308 (2009).
30. Y.-K. Tsang, Nonuniversal velocity probability densities in two-dimensional turbulence: The effect of large-scale dissipation. *Phys. Fluids* **22**, 115102 (2010).
31. M. E. Maltrud, G. K. Vallis, Energy spectra and coherent structures in forced two-dimensional and beta-plane turbulence. *J. Fluid Mech.* **228**, 321–342 (1991).
32. N. Grianik, I. M. Held, K. S. Smith, G. K. Vallis, The effects of quadratic drag on the inverse cascade of two-dimensional turbulence. *Phys. Fluids* **16**, 73–78 (2004).